

Curved Odd Elasticity

Yuan Zhou^{1,*}, Lazaros Tsaloukidis^{2,3,†}, Jack Binysh^{1,‡}, Yuchao Chen,^{4,§} Nikta Fakhri^{4,¶}, Corentin Coulaist^{1,**} and Piotr Surówka^{5,††}

¹*Institute of Physics, University of Amsterdam, Science Park 904, 1098 XH, Amsterdam, The Netherlands*

²*Max Planck Institute for the Physics of Complex Systems, Nöthnitzer Str. 38, 01187, Dresden, Germany*

³*Würzburg-Dresden Cluster of Excellence ct.qmat, 01187, Dresden, Germany*

⁴*Department of Physics, Massachusetts Institute of Technology, Cambridge, MA, USA*

⁵*Institute of Theoretical Physics, Wrocław University of Science and Technology, 50-370 Wrocław, Poland*^{††}

(Dated: December 15, 2025)

Living materials such as membranes, cytoskeletal assemblies, cell collectives and tissues can often be described as active solids—materials that are energized from within, with elastic response about a well defined reference configuration. These materials often live in complex and curved manifolds, yet most descriptions of active solids are flat. Here, we explore the interplay between curvature and non-reciprocal elasticity via a covariant effective theory on curved manifolds in combination with numerical simulations. We find that curvature spatially patterns activity, gaps the spectrum, modifies exceptional points and introduces non-Hermitian defect modes. Together these results establish a foundation for hydrodynamic and rheological models on curved manifolds, with direct implications for living matter and active metamaterials.

Introduction—Many biological and engineered structures—vesicles, cell monolayers, metamaterials—are active solids: materials that are energized from within, with elastic response about a well-defined reference state. Pumping energy into elastic materials brings a range of distinctive phenomena: waves propagate in overdamped media [1–3], modes condense [4–6], topological defects nucleate shape change [7, 8], and solids locomote by themselves [9]. The dominant paradigm in active matter has been fluid-like response, and active stresses that carry an anisotropic order—either polar or nematic [10]. However, recent experiments on e.g. colloids [11], metamaterials [9, 12], spinning embryos [1], or cellular monolayers [13] emphasize chiral active solids as a distinct class of active matter, which features stress propagation without flow, and persistent oscillations. These systems call for complementary elastic descriptions.

In this context, the framework of odd elasticity captures chiral response in a concise and compelling fashion [14–43] (see also [44, 45] for reviews). But odd elasticity is a flat-space theory, and active materials are often curved, especially in biology [Fig. 1(a)]. This curvature matters: curvature-induced distortions can cause localized vibrational modes not present in flat space [46], and topologically enforce defects that act as stress foci [7, 47, 48]. Therefore a central question is: How do odd active crystals interplay with geometry—specifically, how do curvature and topology modify, enable, or suppress the non-reciprocal mechanical responses and collective dynamics which are characteristic of odd elasticity?

Here we develop a covariant low-energy theory of odd elasticity on curved manifolds, complemented by microscopic

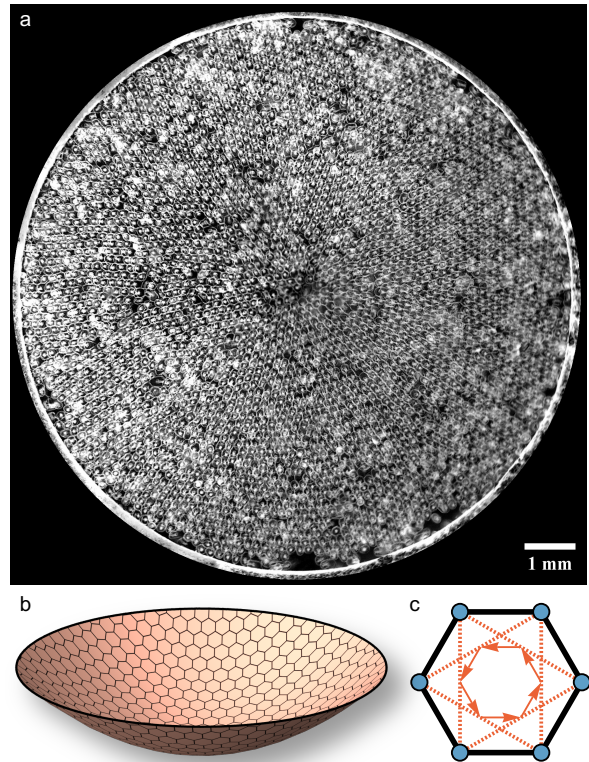


FIG. 1. Curved Odd Elasticity. (a) A living chiral crystal composed of starfish embryos assembled on a curved fluid interface, illustrating an experimental realization of active crystalline order on a curved manifold. (b) Tessellating active plaquettes on curved surfaces provides a minimal model to study how curvature and topology modify non-reciprocal mechanical response. (c) The unit cell of a honeycomb lattice where each bond experiences a non-reciprocal tension-length relationship $T_n = k_o(\Delta_{n+1} - \Delta_{n-1})$, where T_n is the tension in bond n , and Δ_{n+1} , Δ_{n-1} are the length changes in the neighboring bonds $n + 1$ and $n - 1$ within a hexagonal plaquette.

* yzhou@uva.nl

† itsalouk@pks.mpg.de

‡ j.a.c.binysh@uva.nl

§ changyu@mit.edu

¶ fakhri@mit.edu

** coulaist@uva.nl

†† piotr.surwka@pwr.edu.pl

†† LT and YZ contributed equally to this work.

simulations of curved non-reciprocal lattices. Our symmetry-based framework unifies phenomenological theories of defects on curved surfaces [46, 49–58] with the rigorous mathematical theory of shells and thin bodies [59–61], and extends both to non-reciprocal media. We find that curvature gaps complex-frequency modes at long wavelengths, whilst inducing highly localized oscillations around topologically enforced defects. At open boundaries we discover long-wavelength Rayleigh modes that destabilize bulk odd elastic materials from the edge inwards. In a generic curved odd medium, all of these classes of mode exist simultaneously. Our results guide the search for non-reciprocal moduli in complex biomaterials and offer design principles for active metamaterials embedded in our three-dimensional world.

Odd crystallography on curved substrates—Active crystals made of sea-star embryos living at air-water interfaces have been shown to display odd elasticity [1, 62]. These crystals can also live on curved air-water interfaces—menisci [Fig. 1(a)]. Inspired by these systems and by vertex models of curved active solids [7, 63], we construct a microscopic model of active agents with chiral symmetry breaking on a curved substrate. We focus on a minimal model that accounts for self-oscillations while conserving angular momentum: a honeycomb lattice with neighbor interactions that break microscopic reciprocity [Fig. 1(b)]. We endow each edge of our honeycomb with a minimal non-reciprocal tension-length relationship: $T_n = k_o(\Delta_{n+1} - \Delta_{n-1})$, where T_n is the tension in the n^{th} edge, and Δ_{n-1} and Δ_{n+1} measure length changes in the left and right neighboring bonds [Fig. 1(c)]. The passive rigidity of the lattice is ensured by nearest-neighbor springs of stiffness k and next-nearest neighbors of stiffness k' . Many biophysical systems exhibit collective motions confined to a curved substrate [64]. We therefore add strong geometric constraints that confine nodal displacements to the tangent plane of the surface. In flat space, the long-wavelength response of this model has recently been shown to posses odd elastic moduli [43]. How does curvature affect this coarse-grained response?

Curved surfaces bring two ingredients: geometric distortions through a spatially varying metric, and topological constraints through the Euler characteristic. To disentangle these effects we first focus on geometry alone and consider a surface with Euler number zero: a torus [Fig. 2(a)]. Diagonalizing the non-Hermitian dynamical matrix \mathbf{D} of our toroidal lattice, we find complex eigenvalues λ with eigenvectors \mathbf{u} [SM §IV] [43, 65]. We interpret the imaginary component of λ assuming an overdamped dynamics, as is typically the case in biophysical materials [1]. In this context, $\text{Im}(\lambda) \neq 0$ corresponds to oscillations. However, inertial dynamics is also possible [66], in which case $\text{Im}(\lambda) > 0$ implies linear instability. In flat space, the corresponding eigenmodes would be simply periodic [14] and these standing wave modes exhibit consistent strain cycles and energy injection. By contrast, here we find that curvature gives the eigenmodes spatial texture [Fig. 2(a-c)].

To further quantify this spatial structure, we check the local energy injection of each plaquette P_i by calculating the power of internal nonreciprocal bonds $P = \sum_{\text{plaquette}} P_i \propto$

$\text{Im}(\mathbf{u}^\dagger \mathbf{D} \mathbf{u})$. We find a distribution of power injection and dissipation: some hexagonal units have $P_i < 0$ even though the whole system has a net positive power [Fig. 2(c)]. To measure the degree of power reversal in each eigenmode, we sum up the positive $P^+ = \sum(P_i > 0)$ and negative $P^- = \sum(P_i < 0)$ power contributions and introduce the power ratio $p = |P^-|/|P^+|$. We color each mode according to $\log(|1 + p|/|1 - p|)$, which has maximum value when the mode has comparable positive and negative power. In contrast to flat systems, we find that many modes indeed exhibit spatial heterogeneity in their power dissipation—a clear experimentally accessible signature of curvature [Fig. 2(e)]. The question now is how to capture such spatial texture theoretically.

A covariant formulation of odd elasticity—To explain the spatial structure of our eigenmodes, we now develop a framework of curved odd elasticity for a general strain metric. Crystallography on curved manifolds [67] is most naturally formulated in a covariant, two-metric language [49] in which crystalline order spontaneously breaks continuous translations (and rotations). We take a stress-free *reference* metric \bar{g}_{ij} encoding the undeformed lattice and a *dynamical* metric g_{ij} for the deformed configuration, with symmetric strain $u_{ij} = \frac{1}{2}(g_{ij} - \bar{g}_{ij})$. Within this framework, stresses σ^{ab} relate to strains u_{cd} through the elasticity tensor $\sigma^{ab} = C^{abcd}u_{cd}$, and there is a unique covariant extension of the flat-space odd elastic tensor to curved space:

$$C_{\text{odd}}^{abcd} = \frac{K_o}{2} (\bar{g}^{ac}\bar{\epsilon}^{bd} + \bar{g}^{ad}\bar{\epsilon}^{bc} + \bar{g}^{bc}\bar{\epsilon}^{ad} + \bar{g}^{bd}\bar{\epsilon}^{ac}), \quad (1)$$

where $\bar{\epsilon}_{ij}$ is the Levi-Civita tensor density and K_o is the odd modulus. We include this odd contribution directly into the constitutive law built from conservative elasticity [SM §I] and derive the active Navier-Cauchy equations of motion [68]:

$$\begin{aligned} \gamma \frac{\partial u_i}{\partial t} = & \bar{\nabla}_i [(B - \mu) \bar{\nabla}_j u^j + K_o \bar{\epsilon}^{jk} \bar{\nabla}_j u_k] \\ & + \bar{\nabla}_j \bar{\nabla}^j [2\mu u_i + K_o \bar{\epsilon}_i^k u_k] + K_o \bar{\epsilon}_i^k \bar{\nabla}_k (\bar{\nabla}_j u^j), \end{aligned} \quad (2)$$

where $\bar{\nabla}$ is the Levi-Civita connection of \bar{g}_{ij} , and B, μ are the bulk and shear moduli. We illustrate Eq. (2) with an overdamped dynamics γ , but inertial motion is equally possible [9, 66]. Beyond the specific case of odd solids, our covariant two-metric construction provides a minimal and broadly applicable framework for incorporating activity into solid elasticity at the level of constitutive relations (see [SM §I]). In this baseline formulation, non-reciprocal or active effects are captured through generalized material coefficients in the elasticity tensor C^{abcd} , without presupposing additional internal variables, polarity fields, or microstructural order. This does not preclude such fields—which may be essential in more complex active materials—but establishes a geometrically consistent foundation onto which they can be systematically added. Once the reference metric \bar{g}_{ij} and the symmetry class of the solid are specified, the resulting active modifications of the stress-strain relation are encoded directly in the generalized elastic moduli.

We now use the Helmholtz-Hodge decomposition to separate the longitudinal and transverse modes of Eq. (2) into two

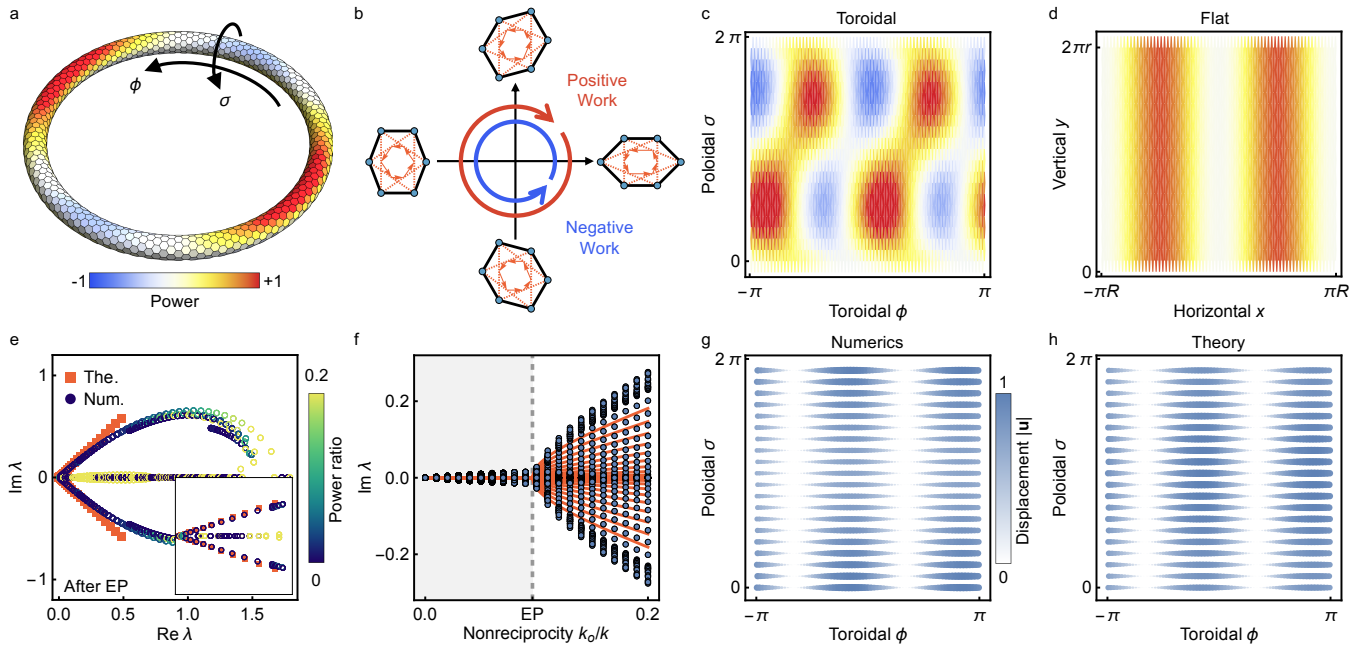


FIG. 2. **Covariant odd elasticity captures the vibrational spectrum of curved non-reciprocal surfaces.** (a, b) An example high-activity bulk mode of a non-reciprocal toroidal lattice. Curvature textures the spatial structure of the modes, creating regions of local power reversal within the lattice in which some plaquettes locally consume energy. (c, d) Regions of power reversal only occur on curved surfaces, not in flat space. (e, f) The vibrational eigenspectrum λ of the lattice is non-Hermitian. Colouring each eigenmode by the power ratio $\log(|1+p|/|1-p|)$, where $p = |P^-|/|P^+|$ quantifies the extent of power reversal, shows that spatial heterogeneity is generic across the spectrum. Our covariant formalism Eq. (3) captures the long-wavelength vibrations of the lattice, and correctly predicts the critical $k_o^*/k = (1+6k'/k)\sqrt{3}/18$ at which the lattice undergoes a bulk exceptional transition and long-wavelength modes become complex. (g, h) Our covariant theory captures not only the eigenvalues λ , but also the spatial structure of the vibrations themselves. Color shows $|\mathbf{u}|$ along the toroidal and poloidal directions for an eigenmode with matched eigenvalue λ between our numerics (g) and theory (h).

potentials, χ and ψ : $u_i = \bar{\nabla}_i \chi + \bar{\epsilon}_{ij} \bar{\nabla}^j \psi$. The dynamics reduces to two coupled scalar equations:

$$\gamma \frac{\partial}{\partial t} \begin{pmatrix} \chi \\ \psi \end{pmatrix} = \bar{\nabla}^2 \begin{pmatrix} B + \mu & -K_o \\ K_o & \mu \end{pmatrix} \begin{pmatrix} \chi \\ \psi \end{pmatrix}. \quad (3)$$

Equation (3) generalizes odd elasticity to any torsionless manifold endowed with a metric-compatible connection. The flat space Laplacian becomes the Laplace-Beltrami operator $\bar{\nabla}^2$, which encodes any curved substrate. The mixing of the scalar potentials χ and ψ through K_o generalizes the hybridization of phonons found in flat space [14]. We now use our theory Eq. (3) to rationalize the vibrational modes of the non-reciprocal torus.

Odd elastic modes of the torus— In the limit of a slender torus with minor radius r much smaller than major radius R , we find an analytical solution for the long wavelength eigen-spectrum of Eq. (3) [SM §III]:

$$\lambda = \frac{B + 2\mu \pm \Delta}{2} \frac{\alpha^2}{r^2(\alpha^2 - 1)} \left(\frac{m^2}{\alpha^2 - 1} + n^2 \right), \quad (4)$$

where m, n label the toroidal wavenumber [69], $\alpha = R/r \gg 1$ is the aspect ratio and $\Delta = (B^2 - 4K_o^2)^{1/2}$. The eigenvalues given by Eq. (4) capture the long-wavelength modes of our numerics [Fig. 2(e)]. We find an exceptional transition

at $\Delta = 0$, at which the coupling matrix Eq. (3) becomes defective and the long-wavelength spectrum becomes complex. In the SM §IV we explicitly coarse grain the elastic moduli of our lattice to predict a threshold non-reciprocity for this transition of $k_o^*/k = \sqrt{3}(1+6k'/k)/18$, in good agreement with the threshold observed in our numerics [Fig. 2(f)]. Our theory not only captures the mode structure of the eigenvalues λ , but also the spatial structure of the eigenvectors \mathbf{u} . For eigenvalues λ matched between theory and numerics, we project our numerical displacement field \mathbf{u} onto the torus, and find good agreement with solutions derived from Eq. (3) [Figs. 2(f, g)]. In conclusion, our covariant theory correctly captures the large scale collective modes of curved odd systems, and provides a theoretical baseline to compare with additional lattice-scale vibrations.

Topological constraints and defects on an odd sphere— Curvature brings not only geometric distortions, but also topological constraints: on surfaces with nonzero Euler characteristic we must find topological defects in our crystallographic lattice. To this end we examine the spectrum of spherical polyhedra with twelve pentagons, formed by meshing an icosahedron. As in the eigenspectrum of a torus [Fig. 2] we see a long wavelength exceptional transition. However, before this transition we observe a new class of instabilities.

We now find thresholdless modes that oscillate for any nonzero k_o [Fig. 3(a, b)] [11, 70]. Measuring the inverse

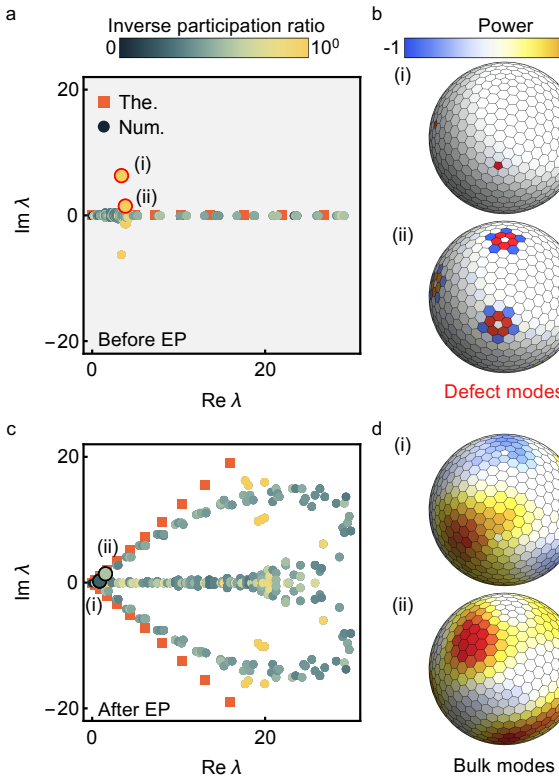


FIG. 3. **Topological constraints on a sphere enforce active defect-bound modes.** (a, b) Defect-bound modes exhibit highly localized strain fields around topologically enforced disclinations. These modes become complex for any nonzero k_0 , well before the bulk exceptional transition. (c, d) Bulk modes display spatially distributed strain fields and are well-described by our theory Eq. (3). This band of continuum modes destabilizes only after the exceptional transition, and merges with the defect-bound modes at large activity.

participation ratio of these modes $\sum_{\text{nodes}} |u_i|^4$, we find that they are highly localized to lattice defects. Before the exceptional transition, strain concentrates at these defects, which serve as local energy sources and dominate the dynamics. After the exceptional transition, bulk modes also become oscillatory [Fig. 3(c, d)]. As k_o increases, these bulk bands eventually merge with the isolated defect-bound modes to once again dominate the eigenspectrum.

To capture the spectrum of the odd sphere at the low-frequency long-wavelength limit we now apply the general framework Eq. (3) to a sphere of radius r [SM §II]. We find that the eigenmodes are spherical harmonics with spectrum

$$\lambda = \frac{B + 2\mu \pm \Delta}{2} \frac{l(l+1)}{r^2}. \quad (5)$$

Finite curvature opens a finite-size gap $\lambda \sim 1/r^2$, which closes as the space tends to be flat $r \rightarrow \infty$, consistent with Goldstone behavior. The analytical prediction also shows a clear level structure that agrees well with our numerical results [Fig. 3(c)]. In summary, curvature simultaneously gaps long-wavelength bulk modes, and introduces highly localized defect-bound states.

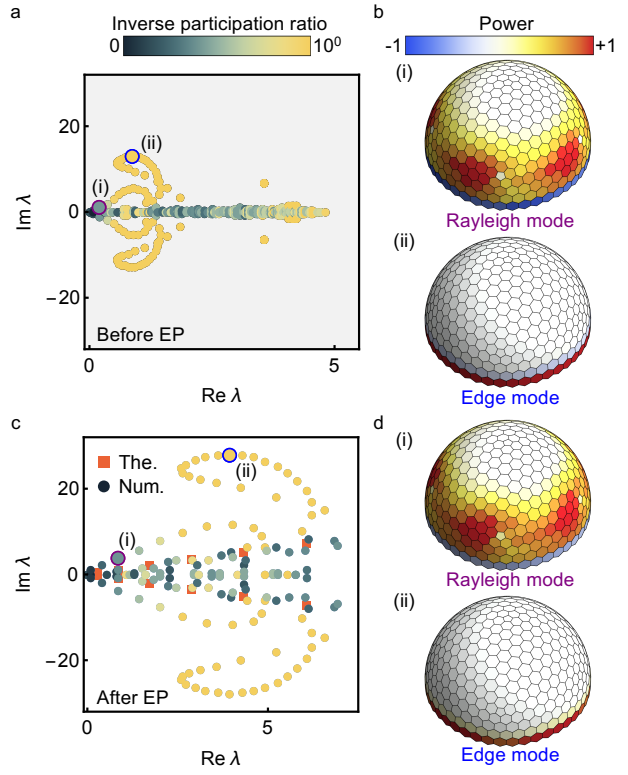


FIG. 4. **Open boundaries create non-Hermitian Rayleigh modes.** (a, b) Cutting a boundary into a spherical cap creates (i) lattice-scale edge modes and (ii) Rayleigh modes with finite penetration depth. Plotting the inverse participation ratio confirms that the low frequency Rayleigh modes are delocalized relative to the edge modes. (c, d) In an open cap defect-bound modes, lattice-scale edge modes and Rayleigh waves all co-exist, each becoming complex before the bulk exceptional transition. Rayleigh modes sit above our theoretically predicted bulk modes even beyond the exceptional transition: the edge is always more unstable than the bulk in odd elastic materials.

Edge modes on a spherical cap— We now consider a final class of mode: boundary states, which play an important role in active systems from topological modes [71, 72] to edge-localized flows [73, 74]. We cut an open boundary into our odd sphere to form a cap [Fig. 4]. Below the bulk exceptional transition we now find two new classes of mode. First are lattice scale edge modes, which have strain cycles localized to the honeycomb plaquettes that form the open boundary itself [Fig. 4(a, b)]. However, in the long-wavelength regime we also find a new band of surface-bound modes with a finite decay length: These are Rayleigh waves. These Rayleigh modes are thresholdless, like our defect-bound modes [Fig. 3(a)]: they cause strong boundary oscillations for any nonzero k_o . However, unlike our defect-bound modes, even beyond the bulk exceptional transition we find that Rayleigh modes sit at $\text{Im}(\lambda)$ values above our theoretically predicted bulk modes for any k_o [Fig. 4(c, d)]: the edge always oscillates more strongly than the bulk.

Discussion— We have built a covariant theory of odd crystals on curved manifolds, complemented by discrete simula-

tions to probe lattice-scale dynamics. Taken together, our results suggest a unified physical picture: activity defines how a solid oscillates, while geometry determines where and in what form it oscillates. In flat living chiral crystals, nonreciprocity partitions the dynamics into acoustic and optical families with characteristic work cycles [62]. On curved manifolds, the same odd-elastic principles combine with Gaussian curvature, defects, and boundaries to orchestrate a broader hierarchy of oscillatory modes, from bulk odd phonons to defect-centered micro-oscillators and boundary-localized Rayleigh waves. This geometric control of oscillatory and work-generating cycles offers predictive design principles for biological tissues, synthetic active metamaterials, and living solids embedded in curved environments.

Looking ahead, the same program that begins with the passive covariant theory of elasticity and extends the equations to include active and odd couplings can be further enriched by torque density terms, Cosserat or micropolar structure, and the inclusion of additional reactive moduli. The continuum theory can also be further generalized to include the out-of-

plane motions when substrate softness is comparable to in-plane stiffness. More broadly, our framework can serve as a foundation for the systematic development of hydrodynamic and rheological models on curved manifolds.

Acknowledgments—We thank Akash Bandhoe and Jonas Veenstra for preliminary numerical explorations and insightful discussions. J.B. acknowledges funding from the European Union’s Horizon research and innovation programme under the Marie Skłodowska-Curie Grant Agreement No. 101106500. C.C. and Y.Z. acknowledge funding from the Netherlands Organization for Scientific Research under grant agreement VI.Vidi.213.131 (C.C. and Y.Z.) and from the European Research Council under grant agreement ERC-CoG 101170693 (C.C.). P.S. was supported in part by the Polish National Science Centre (NCN) Sonata Bis grant 2019/34/E/ST3/00405. L.T. was supported in part by the Deutsche Forschungsgemeinschaft under cluster of excellence ct.qmat (EXC 2147, Project-ID No. 390858490). This work was supported, in part, by the MIT–Poland Lockheed Martin Seed Fund under the MISTI Global Seed Funds program for the project Structural oddities.

[1] T. H. Tan, A. Mietke, J. Li, Y. Chen, H. Higinbotham, P. J. Foster, S. Gokhale, J. Dunkel, and N. Fakhri, Odd dynamics of living chiral crystals, *Nature* **607**, 287 (2022).

[2] H. Xu, Y. Huang, R. Zhang, and Y. Wu, Autonomous waves and global motion modes in living active solids, *Nature Physics* **19**, 46 (2023).

[3] P. Baconnier, O. Dauchot, V. Démery, G. Düring, S. Henkes, C. Huepe, and A. Shee, Self-aligning polar active matter, *Reviews of Modern Physics* **97**, 015007 (2025).

[4] S. Liu, S. Shankar, M. C. Marchetti, and Y. Wu, Viscoelastic control of spatiotemporal order in bacterial active matter, *Nature* **590**, 80 (2021).

[5] P. Baconnier, D. Shohat, C. H. López, C. Coulais, V. Démery, G. Düring, and O. Dauchot, Selective and collective actuation in active solids, *Nature Physics* **18**, 1234 (2022).

[6] F. Gu, B. Guiselin, N. Bain, I. Zuriguel, and D. Bartolo, Emergence of collective oscillations in massive human crowds, *Nature* **638**, 112 (2025).

[7] Y. Maroudas-Sacks, L. Garion, L. Shani-Zerbib, A. Livshits, E. Braun, and K. Keren, Topological defects in the nematic order of actin fibres as organization centres of Hydra morphogenesis, *Nature Physics* **17**, 251 (2021).

[8] F. Brauns, M. O’Leary, A. Hernandez, M. J. Bowick, and M. C. Marchetti, *Active Solids: Topological Defect Self-Propulsion Without Flow* (2025), arXiv:2502.11296 [cond-mat].

[9] J. Veenstra, C. Scheibner, M. Brandenbourger, J. Binysh, A. Souslov, V. Vitelli, and C. Coulais, Adaptive locomotion of active solids, *Nature* **639**, 935 (2025).

[10] S. Shankar, A. Souslov, M. J. Bowick, M. C. Marchetti, and V. Vitelli, Topological active matter, *Nature Reviews Physics* **4**, 380 (2022).

[11] E. S. Bililign, F. Balboa Usabiaga, Y. A. Ganan, A. Poncet, V. Soni, S. Magkiriadou, M. J. Shelley, D. Bartolo, and W. T. M. Irvine, Motile dislocations knead odd crystals into whorls, *Nature Physics* **18**, 212 (2022).

[12] Y. Chen, X. Li, C. Scheibner, V. Vitelli, and G. Huang, Realization of active metamaterials with odd micropolar elasticity, *Nature Communications* **12**, 5935 (2021).

[13] S. Chen, D. E. Gökmen, M. Fruchart, M. Krumbein, P. Silberzan, V. Yashunsky, and V. Vitelli, *Chirality across scales in tissue dynamics* (2025), arXiv:2506.12276 [cond-mat].

[14] C. Scheibner, A. Souslov, D. Banerjee, P. Surówka, W. T. M. Irvine, and V. Vitelli, Odd elasticity, *Nature Physics* **16**, 475 (2020).

[15] D. Banerjee, V. Vitelli, F. Jülicher, and P. Surówka, Active viscoelasticity of odd materials, *Physical Review Letters* **126**, 138001 (2021).

[16] R. Lier, J. Armas, S. Bo, C. Duclut, F. Jülicher, and P. Surówka, Passive odd viscoelasticity, *Phys. Rev. E* **105**, 054607 (2022).

[17] K. Ishimoto, C. Moreau, and K. Yasuda, Odd elastohydrodynamics: Non-reciprocal living material in a viscous fluid, *PRX Life* **1**, 023002 (2023).

[18] P. Surówka, A. Souslov, and D. Banerjee, Odd cosserat elasticity in active materials, *Physical Review E* **108**, 065003 (2023).

[19] S. C. Al-Izzi and G. P. Alexander, Chiral active membranes: Odd mechanics, spontaneous flows, and shape instabilities, *Physical Review Research* **5**, 043227 (2023).

[20] M. Ostoja-Starzewski and P. Surówka, Generalizing odd elasticity theory to odd thermoelasticity for planar materials, *Physical Review B* **109**, 064107 (2024).

[21] P. Matus, R. Lier, and P. Surówka, Molecular modelling of odd viscoelastic fluids, *Physical Review E* **110**, 044605 (2024).

[22] M. Fossati, C. Scheibner, M. Fruchart, and V. Vitelli, Odd elasticity and topological waves in active surfaces, *Physical Review E* **109**, 024608 (2024).

[23] Y.-H. Zhang and Z. Yao, Anisotropic odd elasticity with hamiltonian curl forces, *Journal of Physics A: Mathematical and Theoretical* **57**, 455204 (2024).

[24] L.-S. Lin, K. Yasuda, K. Ishimoto, and S. Komura, Emergence of odd elasticity in a microswimmer using deep reinforcement learning, *Physical Review Research* **6**, 033016 (2024).

[25] A. Lai, J. Zhou, G. Fu, and C. W. Lim, Plane odd elasticity problems: Failure of saint-venant’s principle, *International Journal of Solids and Structures* **319**, 113459 (2025).

[26] A. Lai, K. Wu, J. Zhou, Y. Li, and G. Fu, Nonreciprocal rotating waves of odd elastic circular plates, *Acta Mechanica Solida Sinica* **10**.1007/s10338-025-00606-8 (2025).

[27] A. Lai, Y. Li, and K. Wu, Chiral buckling of odd elastic circular plates, *International Journal of Structural Stability and Dynamics* **10**.1142/S0219455426501750 (2025).

[28] A. Lai, J. Zhou, D. Ou, and K. Wu, Buckling of odd elastic spherical shells, *Thin-Walled Structures* **211**, 113080 (2025).

[29] L. Caprini and U. Marini Bettolo Marconi, Odd active solids: vortices, velocity oscillations and dissipation-free modes, *New Journal of Physics* **27**, 054401 (2025).

[30] L. Quan, S. Yves, Y. Peng, H. Esfahlani, and A. Alù, Odd Willis coupling induced by broken time-reversal symmetry, *Nature Communications* **12**, 2615 (2021).

[31] Q. Wu, P. Shivashankar, X. Xu, Y. Chen, and G. Huang, Engineering nonreciprocal wave dispersion in a nonlocal micropolar metabeam, *Journal of Composite Materials* **57**, 00219983221140562 (2022).

[32] J. Christensen, M. R. Haberman, A. Srivastava, G. Huang, and G. Shmuel, Perspective on non-hermitian elastodynamics, *Applied Physics Letters* **125**, 230501 (2024).

[33] Y. Cohen, A. Schiller, D. Wang, J. A. Dijksman, and M. Moshe, Odd-dipole screening in disordered matter, *Physical Review Materials* **9**, 065602 (2025).

[34] C. Duclut, S. Bo, R. Lier, J. Armas, P. Surówka, and F. Jülicher, Probe particles in odd active viscoelastic fluids: How activity and dissipation determine linear stability, *Physical Review E* **109**, 044126 (2024).

[35] Y. Fu, H. G. E. Hentschel, P. Kaur, A. Kumar, and I. Procaccia, Odd dipole screening in radial inflation, *Physical Review E* **110**, 065003 (2024).

[36] Z. Wolfgram and M. Ostoja-Starzewski, Odd elasticity of cylindrical shells and kirchhoff-love plates under classic continuum theory, *Journal of the Mechanics and Physics of Solids* **185**, 106119 (2025).

[37] M. Ostoja-Starzewski, Thermodynamic basis for odd matter, *Mechanics Research Communications* **10**.1016/j.mechrescom.2025.104488 (2025).

[38] H. Walden, A. Stegmaier, J. Dunkel, and A. Mietke, Odd electrical circuits (2025), arXiv:2503.14383 [cond-mat.soft].

[39] D. Banerjee and P. Sollich, Emergent odd viscoelasticity in chiral soft glassy materials (2025), arXiv:2509.04693 [cond-mat.soft].

[40] C.-T. Lee, T. C. Lubensky, and T. Markovich, Odd elasticity in disordered chiral active materials, arXiv:2508.04468 [cond-mat.soft].

[41] J. Jiang, W. Chen, and M. Amabili, Energy principles for non-Hermitian active metabeams with odd elasticity, *International Journal of Mechanical Sciences* **304**, 110692 (2025).

[42] J. Armas, A. Jain, and R. Lier, Hydrodynamics of thermal active matter, *Physical Review E* **112**, 055401 (2025).

[43] J. Binysh, G. Baardink, J. Veenstra, C. Coulais, and A. Souslov, More is less in unpercolated active solids (2025), arXiv:2504.18362 [cond-mat].

[44] M. Fruchart, C. Scheibner, and V. Vitelli, Odd viscosity and odd elasticity, *Annual Review of Condensed Matter Physics* **14**, 471 (2023).

[45] R. S. Lakes, Colloquium: Materials that exceed classical thermodynamic bounds on properties, *Reviews of Modern Physics* **97**, 021002 (2025).

[46] S. Shankar, M. J. Bowick, and M. C. Marchetti, Topological sound and flocking on curved surfaces, *Physical Review X* **7**, 031039 (2017).

[47] F. C. Keber, E. Loiseau, T. Sanchez, S. J. DeCamp, L. Giomi, M. J. Bowick, M. C. Marchetti, Z. Dogic, and A. R. Bausch, Topology and dynamics of active nematic vesicles, *Science* **345**, 1135 (2014).

[48] T. B. Saw, A. Doostmohammadi, V. Nier, L. Kocgozlu, S. Thampi, Y. Toyama, P. Marcq, C. T. Lim, J. M. Yeomans, and B. Ladoux, Topological defects in epithelia govern cell death and extrusion, *Nature* **544**, 212 (2017).

[49] E. Efrati, E. Sharon, and R. Kupferman, Elastic theory of unconstrained non-Euclidean plates, *Journal of the Mechanics and Physics of Solids* **57**, 762 (2009).

[50] M. Moshe, E. Sharon, and R. Kupferman, Elastic interactions between two-dimensional geometric defects, *Physical Review E* **92**, 062403 (2015).

[51] S. Li, R. Zandi, and A. Travesset, Elasticity in curved topographies: Exact theories and linear approximations, *Physical Review E* **99**, 063005 (2019).

[52] H. Shin, M. J. Bowick, and X. Xing, Topological defects in spherical nematics, *Physical Review Letters* **101**, 037802 (2008).

[53] G. Napoli and L. Vergori, Hydrodynamic theory for nematic shells: The interplay among curvature, flow, and alignment, *Physical Review E* **94**, 020701 (2016).

[54] R. Zhang, Y. Zhou, M. Rahimi, and J. J. de Pablo, Dynamic structure of active nematic shells, *Nature Communications* **7**, 13483 (2016).

[55] S. Henkes, M. C. Marchetti, and R. Sknepnek, Dynamical patterns in nematic active matter on a sphere, *Physical Review E* **97**, 042605 (2018).

[56] K. He, Y. Zhou, and H. Ramezani-Dakhel, From nematic shells to nematic droplets: energetics and defect transitions, *Soft Matter* **18**, 1395 (2022).

[57] G. Napoli, O. V. Pylypovskiy, D. D. Sheka, and L. Vergori, Nematic shells: new insights in topology- and curvature-induced effects, *Soft Matter* **17**, 10322 (2021).

[58] R. Wittmann, L. B. G. Cortes, H. Löwen, and D. G. A. L. Aarts, Particle-resolved topological defects of smectic colloidal liquid crystals in extreme confinement, *Nature Communications* **12**, 623 (2021).

[59] P. G. Ciarlet, *Theory of Shells* (Elsevier, Amsterdam, 2000).

[60] R. D. Kamien, The geometry of soft materials: a primer, *Reviews of Modern Physics* **74**, 953 (2002).

[61] M. J. Bowick and L. Giomi, Two-dimensional matter: order, curvature and defects, *Advances in Physics* **58**, 449 (2009).

[62] Y.-C. Chao, S. Gokhale, L. Lin, A. Hastewell, A. Bacanu, Y. Chen, J. Li, J. Liu, H. Lee, J. Dunkel, and N. Fakhri, Selective excitation of work-generating cycles in nonreciprocal living solids (2024), arXiv:2410.18017 [cond-mat].

[63] D. M. Sussman, Interplay of curvature and rigidity in shape-based models of confluent tissue, *Physical Review Research* **2**, 023417 (2020).

[64] T. Brandstätter, D. B. Brückner, Y. L. Han, R. Alert, M. Guo, and C. P. Broedersz, Curvature induces active velocity waves in rotating spherical tissues, *Nature Communications* **14**, 1643 (2023).

[65] T. C. Lubensky, C. L. Kane, X. Mao, A. Souslov, and K. Sun, Phonons and elasticity in critically coordinated lattices, *Reports on Progress in Physics* **78**, 073901 (2015).

[66] J. Veenstra, J. Binysh, V. Seinen, R. Naber, D. Robledo-Poisson, A. Hunt, W. v. Saarloos, A. Souslov, and C. Coulais, Wave coarsening drives time crystallization in active solids (2025), arXiv:2508.20052 [cond-mat].

[67] V. Vitelli, J. B. Lucks, and D. R. Nelson, Crystallography on curved surfaces, *Proceedings of the National Academy of Sciences USA* **103**, 12323 (2006).

- [68] L. Tsaloukidis, J. J. Fernández-Melgarejo, J. Molina-Vilaplana, and P. Surówka, Fracton-elasticity duality on curved manifolds, [Physical Review B **109**, 085427 \(2024\)](#).
- [69] P. Moon and D. E. Spencer, *Field Theory Handbook: Including Coordinate Systems, Differential Equations and Their Solutions*, 2nd ed. (Springer, Berlin, Heidelberg, 1988).
- [70] L. Braverman, C. Scheibner, B. VanSaders, and V. Vitelli, Topological defects in solids with odd elasticity, [Physical Review Letters **127**, 268001 \(2021\)](#).
- [71] K. Sone, Y. Ashida, and T. Sagawa, Exceptional non-Hermitian topological edge mode and its application to active matter, [Nature Communications **11**, 5745 \(2020\)](#).
- [72] E. Tang, J. Agudo-Canalejo, and R. Golestanian, Topology protects chiral edge currents in stochastic systems, [Physical Review X **11**, 031015 \(2021\)](#).
- [73] C. Scholz, M. Engel, and T. Pöschel, Rotating robots move collectively and self-organize, [Nature Communications **9**, 931 \(2018\)](#).
- [74] Q. Yang, H. Zhu, P. Liu, R. Liu, Q. Shi, K. Chen, N. Zheng, F. Ye, and M. Yang, Topologically protected transport of cargo in a chiral active fluid aided by odd-viscosity-enhanced depletion interactions, [Physical Review Letters **126**, 198001 \(2021\)](#).

Supplementary Material: Curved Odd Elasticity

I. Odd elasticity in curved background

Elasticity on curved backgrounds can be introduced by employing two metrics, $\bar{g}_{\mu\nu}$ and $g_{\mu\nu}$. The first one represents the reference metric, characterizing a strain- and stress free configuration, while the second describes the medium after any deformation applied on it, be it in shape or size. Accordingly, the barred geometric quantities correspond to objects we construct with the reference metric and the unbarred ones to the deformed metric. Based on this definition, the symmetric strain tensor $u_{\alpha\beta}$, is given by the equation:

$$g_{\alpha\beta}(x) = \bar{g}_{\alpha\beta}(x) + 2u_{\alpha\beta} \quad (1)$$

where the Greek indices run from 0 to 2 and the purely time component of the strain tensor is 0 (i.e. $u_{00} = 0$). For now the metric $\bar{g}_{\alpha\beta}(x)$ remains unspecified. We expand the action around it up to the second order perturbatively

$$S[\bar{g} + u] = S[\bar{g}] + \int d^2x dt \sqrt{|\bar{g}|} \left(\frac{\delta S}{\delta \bar{g}_{\alpha\beta}} \right) 2u_{\alpha\beta}(x, t) + \frac{1}{2} \int d^2x d^2x' dt dt' \sqrt{|\bar{g}|} \left(\frac{\delta^2 S}{\delta \bar{g}_{\alpha\beta} \delta \bar{g}_{\gamma\delta}} \right) 4u_{\alpha\beta}u_{\gamma\delta} + \dots \quad (2)$$

The first term on the right hand side is the action coming from the Lagrangian of the undeformed curved solid. This term remains constant with regards to the strain tensor. The first term is vanishing, as the variation with respect to the strain will give the equations of motion for the undeformed solid again. The second term is what represents the generalization of small translations in atom bonds in a curved material, with the term in the parenthesis being equal to the analogue of the rank-4 elastic tensor in curved space. For this we have

$$\frac{\delta^2 S}{\delta \bar{g}_{ab} \delta \bar{g}_{cd}} = \frac{1}{4} (\rho \bar{g}^{ad} \bar{g}^{b0} \bar{g}_0^c - C^{abcd}) \quad (3)$$

with ρ the material density and

$$C^{abcd} = (B - \mu) \bar{g}^{ab} \bar{g}^{cd} + \mu (\bar{g}^{ac} \bar{g}^{bd} + \bar{g}^{bc} \bar{g}^{ad}) \quad (4)$$

for an isotropic solid. This tensor obviously is symmetric under the exchange of the pairs of indices (Maxwell-Betti reciprocity). We also have for the inverse, the analogue generalization of the already familiar expressions

$$(C^{abcd})^{-1} = \left(\frac{1}{4B} - \frac{1}{4\mu} \right) \bar{g}_{ab} \bar{g}_{cd} + \frac{1}{4\mu} (\bar{g}_{ac} \bar{g}_{bd} + \bar{g}_{ad} \bar{g}_{bc}) = \frac{1}{Y} \left[\frac{(1 + \nu)}{2} (\bar{g}_{ac} \bar{g}_{bd} + \bar{g}_{ad} \bar{g}_{bc}) - \nu \bar{g}_{ab} \bar{g}_{cd} \right] \quad (5)$$

and also

$$C^{abcd} C_{cdef} = \frac{1}{2} (\bar{g}_e^a \bar{g}_f^b + \bar{g}_f^a \bar{g}_e^b) \quad (6)$$

where $Y = 2B(1 - \nu) = 2\mu(1 + \nu)$ is the Young's modulus and $\nu = (B - \mu)/(B + \mu)$ is the two dimensional Poisson ratio ranging from -1 for auxetic materials to 1 for fully incompressible solids. Plugging in, the second order action is then given by:

$$S^{2nd} = \frac{1}{2} \int \sqrt{|\bar{g}|} \left[\rho (\bar{\nabla}_0 u^i) (\bar{\nabla}^0 u_i) - C^{abcd} u_{ab} u_{cd} \right] d^2x dt \quad (7)$$

where $\bar{\nabla}_0 = \partial_t$, simply because the curvature distortion does not affect the time component. So we arrive at the elastic action, generalized in a curved background with

$$u_{ab} = \frac{1}{2} (\bar{\nabla}_a u_b + \bar{\nabla}_b u_a) \quad (8)$$

Variation of the action with respect to the strain tensor and the time derivative of the displacement field gives the stress tensor and the momentum density, respectively

$$\begin{aligned} \sigma^{ab} &= \frac{1}{\sqrt{|\bar{g}|}} \frac{\delta S}{\delta u_{ab}} = C^{abcd} u_{cd}, \\ \pi^a &= \frac{1}{\sqrt{|\bar{g}|}} \frac{\delta S}{\delta (\partial_t u_a)} = \rho (\partial_0 u^a) \end{aligned} \quad (9)$$

In order to derive our equation of motion we will be performing a variation of the action, which after a small and straightforward calculation leads to

$$\delta S = - \int \sqrt{|\bar{g}|} [\rho \partial_t^2 u^a - C^{abcd} \bar{\nabla}_b \bar{\nabla}_c u_d] (\delta u_a) d^2 x dt \quad (10)$$

The next step is the extension of the rank-4 tensor with the odd elastic terms related to the modulus K_o . In principle the inclusion of the odd modulus A is also possible for a solid with internal torque density, but we choose not to for simplicity. This term in curved background is given from:

$$C_{odd}^{abcd} = \frac{K_o}{2} (\bar{g}^{ac} \bar{\epsilon}^{bd} + \bar{g}^{ad} \bar{\epsilon}^{bc} + \bar{g}^{bc} \bar{\epsilon}^{ad} + \bar{g}^{bd} \bar{\epsilon}^{ac}) \quad (11)$$

where in our case $\bar{\epsilon}^{ab} = \epsilon^{ab} / \sqrt{|\bar{g}|}$ ¹. The final result is the odd Navier's equation for the displacement field

$$\rho \frac{\partial^2 u_i}{\partial t^2} - \bar{\nabla}_i \left[(B - \mu) (\bar{\nabla}_j u_j) + \frac{K_o}{\sqrt{|\bar{g}|}} (\epsilon_{jk} \bar{\nabla}_j u_k) \right] - \bar{\nabla}_j^2 \left[2\mu u_i + \frac{K_o}{\sqrt{|\bar{g}|}} (\epsilon_{ik} u_k) \right] - \frac{K_o}{\sqrt{|\bar{g}|}} \epsilon_{ik} \bar{\nabla}_k (\bar{\nabla}_j u_j) = 0 \quad (12)$$

The structure of the above second-order, coupled linear equations makes finding closed-form solutions particularly challenging. To address this, we introduce two scalar functions (Papkovich–Neuber potentials):

$$u_i = \bar{\nabla}_i \chi + \bar{\epsilon}_{ij} \bar{\nabla}^j \psi. \quad (13)$$

Substituting this representation into the governing equations yields the following form:

$$\bar{\nabla}_i \left[\rho \frac{\partial^2 \chi}{\partial t^2} - (B + \mu) \bar{\nabla}^2 \chi + K_o \bar{\nabla}^2 \psi \right] + \epsilon_{ik} \bar{\nabla}^k \left[\rho \frac{\partial^2 \psi}{\partial t^2} - \mu \bar{\nabla}^2 \psi - K_o \bar{\nabla}^2 \chi \right] = 0.$$

This expression can be satisfied only if²:

$$\rho \frac{\partial^2 \chi}{\partial t^2} - (B + \mu) \bar{\nabla}^2 \chi + K_o \bar{\nabla}^2 \psi = 0, \quad (14)$$

and

$$\rho \frac{\partial^2 \psi}{\partial t^2} - \mu \bar{\nabla}^2 \psi - K_o \bar{\nabla}^2 \chi = 0. \quad (15)$$

These coupled linear differential equations written in general curvilinear coordinates also provide the usual solutions for the modes for the case of 2D flat surface (infinitely long plate). In the case where $K_o = 0$, we also recover back the usual solutions for the passive elastic solid. In the next sections we will be applying all our results to the cases of a spherical and a toroidal surface.

II. Application on the 2-sphere

For the case of a 2-sphere of radius r , polar angle θ and azimuthal angle ϕ ,

$$\begin{aligned} x &= r \sin \theta \cos \phi, \\ y &= r \sin \theta \sin \phi, \\ z &= r \cos \theta. \end{aligned} \quad (16)$$

where we want to apply our findings, we have

$$\begin{aligned} \bar{g}_{ab}(x) &= \begin{pmatrix} r^2 & 0 \\ 0 & r^2 \sin^2 \theta \end{pmatrix}, \\ \bar{g}^{ab}(x) &= \begin{pmatrix} \frac{1}{r^2} & 0 \\ 0 & \frac{1}{r^2 \sin^2 \theta} \end{pmatrix}. \end{aligned} \quad (17)$$

¹ If we include the odd contribution before the covariant derivative bypasses the rank-4 elasticity tensor during the extraction of the equation of motion, it would still have no difference in the final result as $\bar{\nabla}_\alpha \sqrt{|\bar{g}|} = 0$.

² We clarify that every solution of the Navier's equation admits a representation like the one provided by Eq. 13.

At the same time for the Ricci scalar and the square root of the metric determinant

$$\mathcal{R} = \frac{2}{r^2}, \quad \sqrt{|\bar{g}|} = r^2 \sin \theta. \quad (18)$$

We will be also introducing now a damping effect, directly in the equations of motion for the scalar potentials through a first order time derivative, multiplied by the positive parameter γ , which regulates the energy loss rate of the system.

$$\begin{aligned} \rho \frac{\partial^2 \chi}{\partial t^2} + \gamma \frac{\partial \chi}{\partial t} - (B + \mu) \bar{\nabla}_j^2 \chi + K_o \bar{\nabla}_j^2 \psi &= 0 \\ \rho \frac{\partial^2 \psi}{\partial t^2} + \gamma \frac{\partial \psi}{\partial t} - \mu \bar{\nabla}_j^2 \psi - K_o \bar{\nabla}_j^2 \chi &= 0 \end{aligned} \quad (19)$$

By making use of the Laplace–Beltrami operator on a two-dimensional sphere of fixed radius r ,

$$\bar{\nabla}^2 = \frac{1}{r^2} \left[\frac{\partial^2}{\partial \theta^2} + \cot \theta \frac{\partial}{\partial \theta} + \frac{1}{\sin^2 \theta} \frac{\partial^2}{\partial \phi^2} \right], \quad (20)$$

and expanding the scalar potentials in spherical time harmonics,

$$\begin{aligned} \chi(\theta, \phi, t) &= \sum_{l=0}^{\infty} \sum_{m=-l}^l C_{lm} Y_l^m(\theta, \phi) e^{i\omega t}, \\ \psi(\theta, \phi, t) &= \sum_{l=0}^{\infty} \sum_{m=-l}^l D_{lm} Y_l^m(\theta, \phi) e^{i\omega t}, \end{aligned} \quad (21)$$

where C_{lm} and D_{lm} depend on the mode numbers (l, m) , we use the eigenvalue relation

$$r^2 \bar{\nabla}^2 Y_l^m(\theta, \phi) = -l(l+1) Y_l^m(\theta, \phi), \quad (22)$$

together with the completeness relation

$$\int_0^{2\pi} \int_0^\pi Y_l^m(\theta, \phi) (Y_{l'}^{m'}(\theta, \phi))^* \sin \theta d\theta d\phi = \delta_{l,l'} \delta_{m,m'}. \quad (23)$$

Projecting the governing equations onto this orthonormal basis yields, for each mode (l, m) , the 2×2 matrix system

$$\begin{pmatrix} \rho \omega^2 - i\gamma\omega - \frac{(B + \mu)}{r^2} l(l+1) & \frac{K_o}{r^2} l(l+1) \\ -\frac{K_o}{r^2} l(l+1) & \rho \omega^2 - i\gamma\omega - \frac{\mu}{r^2} l(l+1) \end{pmatrix}. \quad (24)$$

Setting the determinant of the above matrix equal to zero yields a quartic (characteristic polynomial of rank 4) of the form

$$\omega^4 + A \omega^3 + B \omega^2 + C \omega + D = 0, \quad (25)$$

where

$$\begin{aligned} A &= -2i \frac{\gamma}{\rho}, \\ B &= -\frac{\rho(B + 2\mu) l(l+1) + \gamma^2 r^2}{\rho^2 r^2}, \\ C &= 2i \frac{\gamma(B + 2\mu) l(l+1)}{\rho^2 r^2}, \\ D &= \frac{\mu(B + \mu) + K_o^2}{\rho^2 r^4} l^2(l+1)^2. \end{aligned} \quad (26)$$

Solving this quartic for the frequency yields the four eigenvalues

$$\omega_\gamma = i \frac{\gamma}{2\rho} \pm \frac{1}{r} \sqrt{\frac{[(B+2\mu) \pm \sqrt{B^2 - 4K_o^2}] l(l+1) - \frac{\gamma^2 r^2}{2}}{2\rho_d}}. \quad (27)$$

In the limit where $\gamma = 0$, The modal solutions come out as

$$\omega_l^2 = \frac{B+2\mu \pm \sqrt{B^2 - 4K_o^2}}{2\rho} \frac{l(l+1)}{r^2} \quad (28)$$

The spectrum is inversely proportional to r^2 . The flat limit for the 2D infinitely long odd plate can in principle be recovered if the fraction of l^2/r^2 for large l is instead replaced for the k^2 of the wavenumber for the linear spectrum of the continuum limit.

In the overdamped regime on the other hand ($\rho \ll \gamma$), the above polynomial simplifies into

$$\omega^2 - i \frac{(B+2\mu)l(l+1)}{\gamma r^2} \omega - \frac{[\mu(B+\mu) + K_o^2]}{\gamma^2 r^4} l^2(l+1)^2 = 0$$

with solution

$$\omega_\gamma^{\text{over}} = i \frac{(B+2\mu) \pm \sqrt{B^2 - 4K_o^2}}{2\gamma} \frac{l(l+1)}{r^2}. \quad (29)$$

The spectrum now is inversely proportional to r^2 and quadratically dependent on the quadratic in the angular mode index l . It is clear from Eq. (29) that just like the infinitely long plate theory, wave solutions can still be present in the overdamped case where $4K_o^2 > B^2$ as now $\omega_\gamma^{\text{over}}$ acquires a real part.

The corresponding eigenvector is

$$\begin{pmatrix} C_{lm} \\ D_{lm} \end{pmatrix} = \begin{pmatrix} B \pm \sqrt{B^2 - 4K_o^2} \\ 2K_o \end{pmatrix}. \quad (30)$$

The displacement fields follow from the Papkovich–Neuber representation,

$$u_i = \bar{\nabla}_i \chi + \bar{\epsilon}_{ij} \bar{\nabla}^j \psi = \left(\frac{1}{r} \frac{\partial \chi}{\partial \theta} + \frac{1}{r \sin \theta} \frac{\partial \psi}{\partial \phi}, \frac{1}{r \sin \theta} \frac{\partial \chi}{\partial \phi} - \frac{1}{r} \frac{\partial \psi}{\partial \theta} \right), \quad (31)$$

where the two components correspond to the θ and ϕ directions on the sphere.

The resulting mode therefore takes the form

$$\mathbf{u}_l^m = \left(\frac{C_{lm}}{r} \frac{\partial}{\partial \theta} + \frac{D_{lm}}{r \sin \theta} \frac{\partial}{\partial \phi}, \frac{C_{lm}}{r \sin \theta} \frac{\partial}{\partial \phi} - \frac{D_{lm}}{r} \frac{\partial}{\partial \theta} \right) P_l^m(\cos \theta) e^{im\phi} e^{i\omega_l t}, \quad (32)$$

where $P_l^m(\cos \theta)$ denotes the associated Legendre polynomial.

III. Application on a toroidal surface

The torus formed when rotating around the axis z , a ring of radius r , whose center lies in the xy plane, a distance R from point $(0, 0, 0)$, can be parametrized as

$$\begin{aligned} x &= (R + r \cos \theta) \cos \phi, \\ y &= (R + r \cos \theta) \sin \phi, \\ z &= r \sin \theta, \end{aligned} \quad (33)$$

where $R > 0, r > 0, -\pi \leq \phi, \theta \leq \pi$, or

$$\begin{aligned} x &= a \frac{\sinh \tau}{\cosh \tau - \cos \sigma} \cos \phi, \\ y &= a \frac{\sinh \tau}{\cosh \tau - \cos \sigma} \sin \phi, \\ z &= a \frac{\sin \sigma}{\cosh \tau - \cos \sigma}, \end{aligned} \quad (34)$$

where the coordinate ranges are $a > 0, \tau > 0, -\pi \leq \phi, \sigma \leq \pi$. The geometric parameters are

$$\begin{aligned} R &= a \coth \tau, \quad r = a \operatorname{csch} \tau, \\ a &= \sqrt{R^2 - r^2}, \quad \tau = \log \left(\frac{R}{r} + \sqrt{\frac{R^2}{r^2} - 1} \right). \end{aligned} \quad (35)$$

The area of a torus is $A = 4\pi^2 Rr = 4\pi^2 a^2 \coth \tau \operatorname{csch} \tau$.

We choose to work here with the second option for the modal solutions. The metric tensor and its inverse for a toroid (also called a 2-Torus), is given by

$$\begin{aligned} \bar{g}_{ij} &= \begin{pmatrix} \frac{a^2 \sinh^2 \tau}{(\cosh \tau - \cos \sigma)^2} & 0 \\ 0 & \frac{a^2}{(\cosh \tau - \cos \sigma)^2} \end{pmatrix}, \\ \bar{g}^{ij} &= \begin{pmatrix} \frac{(\cosh \tau - \cos \sigma)^2}{a^2 \sinh^2 \tau} & 0 \\ 0 & \frac{(\cosh \tau - \cos \sigma)^2}{a^2} \end{pmatrix}, \end{aligned} \quad (36)$$

and appropriately, we can define the Laplace-Beltrami operator

$$\bar{\nabla}^2 = \frac{(\cosh \tau - \cos \sigma)^2}{a^2} \left(\frac{1}{\sinh^2 \tau} \frac{\partial^2}{\partial \phi^2} + \frac{\partial^2}{\partial \sigma^2} \right). \quad (37)$$

To make things simpler, we will choose to work on a toroid where the radius from the center is much bigger than the internal radius of the ring, i.e. $R \gg r$. In that approximation, the $\cos \sigma$, can be dropped and we can use the simple ansatz for the general solution of the scalar potentials

$$\begin{aligned} \chi(\phi, \sigma) &\sim \tilde{\chi} e^{im\phi} e^{in\sigma}, \\ \psi(\phi, \sigma) &\sim \tilde{\psi} e^{im\phi} e^{in\sigma}. \end{aligned} \quad (38)$$

The eigenvalue problem takes the form

$$-\rho \omega^2 \begin{pmatrix} \tilde{\chi} \\ \tilde{\psi} \end{pmatrix} = -\frac{\cosh^2 \tau}{a^2} \left(\frac{m^2}{\sinh^2 \tau} + n^2 \right) \begin{pmatrix} B + \mu & -K^o \\ K^o & \mu \end{pmatrix} \begin{pmatrix} \tilde{\chi} \\ \tilde{\psi} \end{pmatrix}, \quad (39)$$

with eigen-frequencies

$$\omega^2 = \frac{B + 2\mu \pm \sqrt{B^2 - 4K^o}}{2\rho} \frac{\cosh^2 \tau}{a^2} \left(\frac{m^2}{\sinh^2 \tau} + n^2 \right). \quad (40)$$

In the limit $R/r \rightarrow \infty$, the equation reduces to that of a cylindrical surface:

$$\omega^2 = \frac{B + 2\mu \pm \sqrt{B^2 - 4K^o}}{2\rho} \frac{n^2}{r^2}. \quad (41)$$

The eigenvector is

$$\begin{pmatrix} \tilde{\chi} \\ \tilde{\psi} \end{pmatrix} = \begin{pmatrix} B \pm \sqrt{B^2 - 4K^o} \\ 2K^o \end{pmatrix} \quad (42)$$

The displacement fields read

$$u_i = \bar{\nabla}_i \chi + \bar{\epsilon}_{ij} \bar{\nabla}^j \psi = \frac{\cosh \tau - \cos \sigma}{a} \left(\frac{1}{\sinh \tau} \frac{\partial \chi}{\partial \phi} + \frac{\partial \psi}{\partial \sigma}, \frac{\partial \chi}{\partial \sigma} - \frac{1}{\sinh \tau} \frac{\partial \psi}{\partial \phi} \right), \quad (43)$$

and the mode is

$$\mathbf{u}_{m,n} = \frac{\cosh \tau - \cos \sigma}{a} \left(\frac{\tilde{\chi}}{\sinh \tau} \frac{\partial}{\partial \phi} + \tilde{\psi} \frac{\partial}{\partial \sigma}, \tilde{\chi} \frac{\partial}{\partial \sigma} - \frac{\tilde{\psi}}{\sinh \tau} \frac{\partial}{\partial \phi} \right) e^{im\phi} e^{in\sigma} e^{i\omega_{m,n} t}. \quad (44)$$

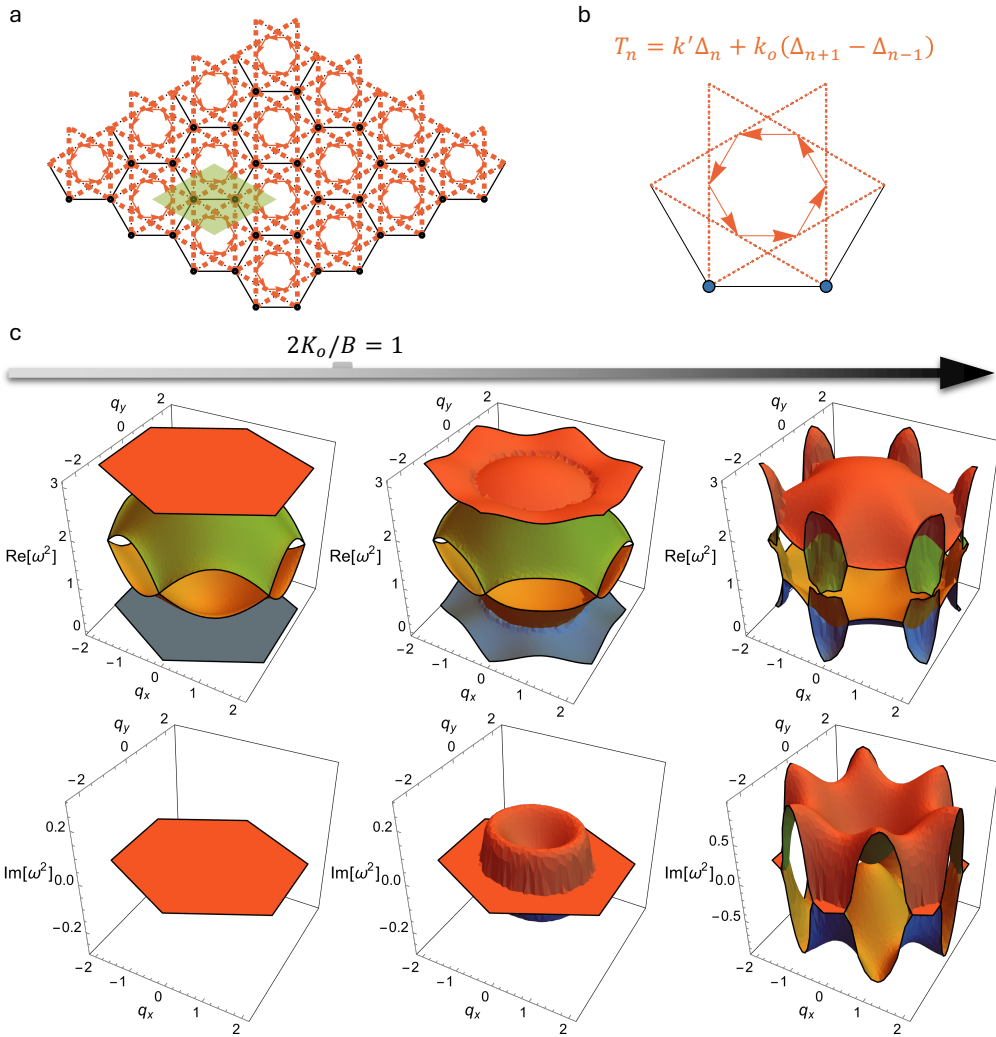


FIG. 1. Band structure of a flat honeycomb lattice. (a) A honeycomb lattice. (b) The unit cell with nonreciprocal next-nearest interactions. (c) The spectrum plotted over the Brillouin zone for $k_o/k = 0, 0.16, 0.4$.

IV. Microscopic lattices

Here we consider a honeycomb lattice with next-nearest neighboring nonreciprocal interactions [Figs. 1(a, b)]

$$T_n = k' \Delta_n + k_o (\Delta_{n+1} - \Delta_{n-1}), \quad (45)$$

where Δ_n, T_n denote bond elongation and tension, k', k_o represent reciprocal and nonreciprocal stiffness. The linear dynamics are governed by the equation of motion

$$\mathbf{M}\ddot{\mathbf{u}} = \mathbf{F} = -\mathbf{D}\mathbf{u} = -\mathbf{C}^T \mathbf{K} \mathbf{C} \mathbf{u}, \quad (46)$$

where \mathbf{M} is the diagonal matrix of nodal mass, and \mathbf{D} is the dynamical matrix. The geometric information is encoded by the compatibility matrix \mathbf{C} , and the elastic interactions are assembled into the stiffness matrix \mathbf{K} . It is a diagonal matrix $\text{diag}(k_1, k_2, \dots, k_{N_b}, k'_1, k'_2, \dots, k'_{N_{N_b}})$ in reciprocal systems, while nonreciprocal interactions introduce antisymmetric terms k_o .

For periodic lattices, we can take the Fourier transform of Eq. (46)

$$-\mathbf{M}\omega^2 \tilde{\mathbf{u}} = -\mathbf{C}^\dagger(\mathbf{q}) \mathbf{K} \mathbf{C}(\mathbf{q}) \tilde{\mathbf{u}}, \quad (47)$$

where \mathbf{q} is the wave-vector. The band structure can be solved from the equation by calculating the eigenvalues for each wave-vector at the Brillouin zone. We find the real bands become complex at a critical nonreciprocal stiffness [Fig. 1(c)], a typical

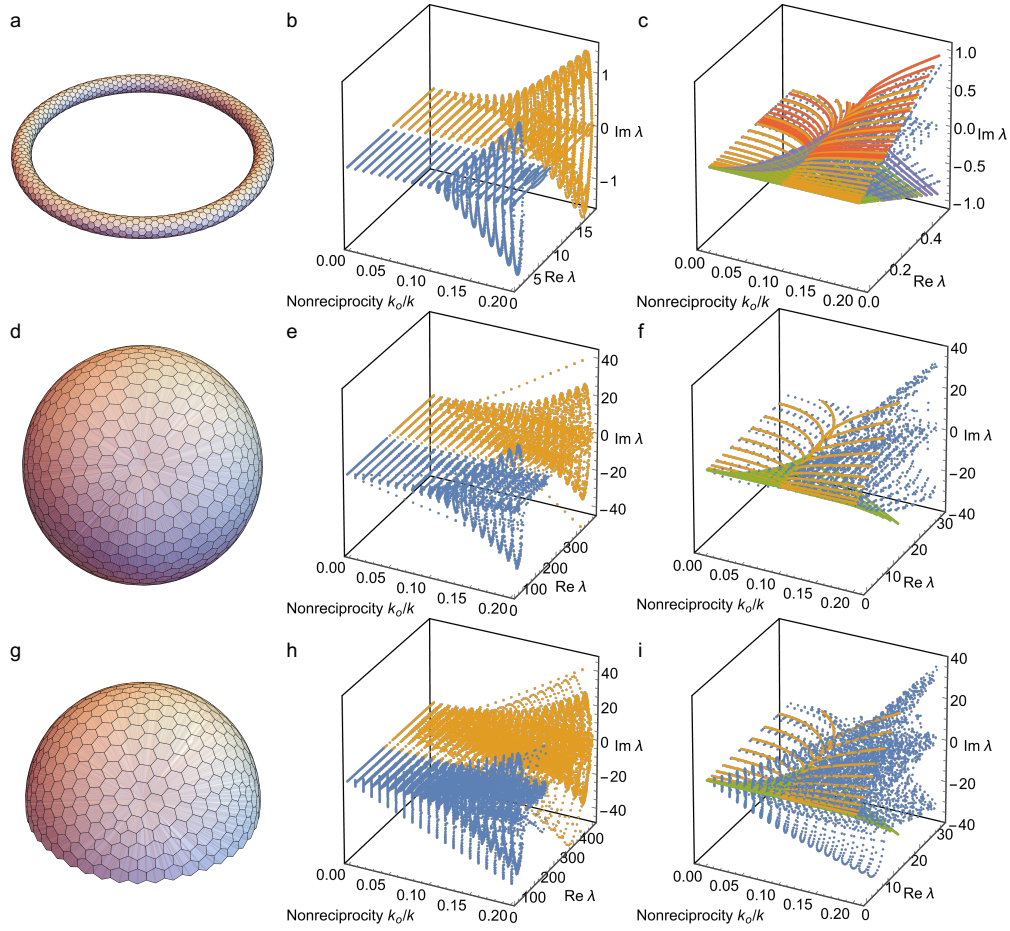


FIG. 2. Vibrational spectra of curved systems. (a, d, g) A torus, full spherical surface, and a half-spherical cap. (b, e, h) The $2N$ in-plane optical and acoustic branches. (c, f, i) The low-frequency spectra and theoretical predictions of curved odd elasticity. (c) The yellow and orange branches ($m = 1, 2, \dots$) denote λ_+ with $n = 0$ and $n = 1$. The green and purple branches denote λ_- with $n = 0$ and $n = 1$. (f, i) The yellow and green branches ($l = 1, 2, \dots$) denote λ_+ and λ_- , respectively.

feature of exceptional transition. Interestingly, the instability appears first at the long-wavelength limit and gradually immerse the whole Brillouin zone.

Following a standard coarse graining procedure [43, 65], we extract the isotropic elastic modulus tensor for the nonreciprocal honeycomb lattice. We choose the four basis for second-order tensor

$$\tau^0 = \begin{pmatrix} 1 & 0 \\ 0 & 1 \end{pmatrix}, \quad \tau^1 = \begin{pmatrix} 0 & -1 \\ 1 & 0 \end{pmatrix}, \quad \tau^2 = \begin{pmatrix} 1 & 0 \\ 0 & -1 \end{pmatrix}, \quad \tau^3 = \begin{pmatrix} 0 & 1 \\ 1 & 0 \end{pmatrix}, \quad (48)$$

and the constitutive equation is expressed in the matrix form

$$\begin{pmatrix} \sigma^0 \\ \sigma^1 \\ \sigma^2 \\ \sigma^3 \end{pmatrix} = 2 \begin{pmatrix} B & 0 & 0 & 0 \\ 0 & 0 & 0 & 0 \\ 0 & 0 & \mu & K_o \\ 0 & 0 & -K_o & \mu \end{pmatrix} \begin{pmatrix} u^0 \\ u^1 \\ u^2 \\ u^3 \end{pmatrix} \quad (49)$$

where bulk modulus, shear modulus, and odd modulus are

$$B = \frac{k + 6k'}{2\sqrt{3}}, \quad \mu = \frac{\sqrt{3}k'}{2}, \quad K_o = \frac{3k_o}{2}. \quad (50)$$

V. Curved systems

For our curved systems, we introduce another strong geometric constraints k_c that confine nodal displacements to the tangent plane. Specifically, we introduce springs with stiffness k_c to connect each node (x, y, z) on surfaces to the axial circle $(R \cos \phi, R \sin \phi, 0)$ of a torus or the origin $(0, 0, 0)$ of a spherical surface. In the following analysis, we set the stiffness $k_c/k = 10^4$ to impose strong constraints, $k'/k = 10^{-4}$ to introduce nonzero shear modulus, and $k_o/k \sim 1$ to capture the odd effects.

For a curved system consisting of N nodes, there are $3N$ degrees of freedom. The out-of-plane responses exhibit N high frequencies $\omega^2 \sim k_c/m_a$, and the in-plane motions are composed with the optical and acoustic branches, as the band structure of the diatomic honeycomb lattice shown in Figs. 1(b, c). Furthermore, the acoustic branch consists of longitudinal $\omega^2 \sim k/m_a$ and transverse $\omega^2 \sim k'/m_a$ sections in passive systems, which are involved with the bulk and shear moduli in the continuum limit. The existence of nonreciprocal interactions mix the longitudinal and transverse components and therefore lead to chiral phonons. The vibrational spectra of curved system are shown in Fig. 2. To compare with the analytical predictions, we calculate the density of each curved lattice $\rho = Nm_a/A$, where A is the area of a torus $4\pi^2 Rr$, a spherical surface $4\pi r^2$, or a half-spherical cap $2\pi r^2$.

To characterize energy injection in curved systems, we evaluate the power associated with each eigenmode,

$$P = \text{Re} \langle \mathbf{u} | \mathbf{F} \rangle = \text{Re}(-i\omega \mathbf{u}^\dagger \mathbf{C}^T \mathbf{K} \mathbf{C} \mathbf{u}) = \omega \text{Im}(\mathbf{u}^\dagger \mathbf{C}^T \mathbf{K} \mathbf{C} \mathbf{u}) = \omega \text{Im}(\mathbf{u}^\dagger \mathbf{C}^T \mathbf{K}_o \mathbf{C} \mathbf{u}) \quad (51)$$

In nonreciprocal systems, the stiffness matrix contains antisymmetric components. These antisymmetric contributions generate nonzero local power on each plaquette, so that the total power can be written as $P = \sum_{\text{plaquette}} P_i$. We therefore color each hexagonal units to visualize the distribution and identify power reversals. To globally measure the degree of power reversal in each eigenmode, we sum up the positive $P^+ = \sum(P_i > 0)$ and negative $P^- = \sum(P_i < 0)$ power contributions and introduce the power ratio $p = |P^-|/|P^+|$.